CrossMark

A Local Approximation of Fundamental Measure Theory Incorporated into Three Dimensional Poisson–Nernst–Planck Equations to Account for Hard Sphere Repulsion Among Ions

Yu Qiao[1] · Xuejiao Liu[1] · Minxin Chen [2] ·
Benzhuo Lu[1]

Abstract The hard sphere repulsion among ions can be considered in the Poisson–Nernst–Planck (PNP) equations by combining the fundamental measure theory (FMT). To reduce the nonlocal computational complexity in 3D simulation of biological systems, a local approximation of FMT is derived, which forms a local hard sphere PNP (LHSPNP) model. In the derivation, the excess chemical potential from hard sphere repulsion is obtained with the FMT and has six integration components. For the integrands and weighted densities in each component, Taylor expansions are performed and the lowest order approximations are taken, which result in the final local hard sphere (LHS) excess chemical potential with four components. By plugging the LHS excess chemical potential into the ionic flux expression in the Nernst–Planck equation, the three dimensional LHSPNP is obtained. It is interestingly found that the essential part of free energy term of the previous size modified model (Borukhov et al. in Phys Rev Lett 79:435–438, 1997; Kilic et al. in Phys Rev E 75:021502, 2007; Lu and Zhou in Biophys J 100:2475–2485, 2011; Liu and Eisenberg in J Chem Phys 141:22D532, 2014) has a very similar form to one term of the LHS model, but LHSPNP has more additional terms accounting for size effects. Equation of state for one component homogeneous fluid is studied for the local hard sphere approximation of FMT and is proved to be exact for the first two virial coefficients, while the previous size modified model only presents the first virial coefficient accurately. To investigate the effects of LHS model and the competitions among different counterion species, numerical experiments are performed for the traditional PNP model, the LHSPNP model, the previous size modified PNP (SMPNP) model and the Monte Carlo simulation. It's observed that in steady state the LHSPNP results are quite different from the PNP results, but are close to the SMPNP results under a wide range of boundary

✉ Benzhuo Lu
  bzlu@lsec.cc.ac.cn

[1] State Key Laboratory of Scientific and Engineering Computing, National Center for Mathematics and Interdisciplinary Sciences, Academy of Mathematics and Systems Science, Chinese Academy of Sciences, Beijing 100190, China

[2] Department of Mathematics, Center for System Biology, Soochow University, Suzhou 215006, China

conditions. Besides, in both LHSPNP and SMPNP models the stratification of one counterion species can be observed under certain bulk concentrations.

Keywords Hard sphere repulsion · Three dimensional fundamental measure theory · Poisson–Nernst–Planck equations · Size-modified PNP · Equation of state

1 Introduction

In systems of charged particles, the traditional continuum Poisson–Nernst–Planck (PNP) model has been widely used for modeling and simulating a variety of interesting phenomena, such as ion distributions around charged particles [2,43,44], and flow of ions across channels [1,9,19,25,27,35,68] and axons [49]. A defect in the PNP model is the point charge treatment of ions which in fact have finite volumes. This may lead to unphysical concentration values in the neighborhood of biomolecules [6,43,50] and hence can not properly capture the size effects which may play important role in ion permeation through ion channels.

A great deal of efforts have been devoted to remedy this disadvantage and improve the PNP model to provide reliable predictions through including ionic size effects and ion-ion correlations. In equilibrium and uniform ionic size, Andelman et al. have incorporated the ionic size effects into the traditional continuum model, and provided the explicit expressions of ion concentrations and the uniform size modified Poisson–Boltzmann (SMPB) equation [6,7]. This is derived by introducing an additional solvent entropy term, representing the unfavorable energy modeling the overpacking or crowding of ions and solvent molecules, into the free energy form. Fenley's group has studied this SMPB model explicitly through comparisons with the original Poisson–Boltzmann (PB) model, and investigations of the sensitivities to parameterization [23,24,64]. By using a rigorous lattice gas method, Chu et al. extended this uniform SMPB model to make it work for two different ion sizes and studied ion binding to DNA duplexes which showed improved agreements with experimental data [12]. In the case of three or more different sizes, the rigorous lattice gas method is hard to apply to give an explicit SMPB equation, but an alternative size modified Poisson–Nernst–Planck (SMPNP) model is derived in our previous work which can be considered as an implicit SMPB model in equilibrium [43,50]. Li et al. have provided some mathematical analysis on the energy functional for the SMPB model [37]. In recent work by Liu and Eisenberg [39–41], they considered the size effects from all spherical ions, water molecules (treated as polarizable spheres) and interstitial voids, and derived an entropy form of those spheres of arbitrary diameter and voids. To further account for the correlation effect of ions, Liu and Eisenberg's work also included a high-order derivative term of potential in free energy functional derived by Santangelo [61] which has similar form to Cahn–Hilliard concentration-gradient expansions [8,47]. The resulted fourth order Poisson–Fermi equation [40,41] (for equilibrium condition) and Poisson–Nernst–Planck–Fermi equations (for nonequilibrium condition) [41] can account for the steric effect of ions and water molecules, the correlation effect of crowded ions, the screening effect of polar water, as well as the charge/space competition effect of ions and water molecules. These models were shown to be able to capture critical phenomena such as ion binding, blocking, and selective permeation of L-type calcium channels [39–41].

Apart from the above mean field modified models, coupling of density functional theory (DFT) and PNP model has also been used to account for ion-ion interactions in solutions. The major description of DFT lies in the construction of the excess Helmholtz free energy [14]. Rosenfeld derived the fundamental measure theory (FMT) to express the excess Helmholtz free energy for hard sphere mixtures [51], which contains four scalar and two vector weight

functions, and has been widely used in many literatures [15,16,19,22,28,29,31,32,34,36, 38,42,46,48,52–60,62,65–67,70]. Not long after that, he extended the original FMT, that works for three dimensional inhomogeneous fluids, to predict a freezing transition of the hard-sphere fluid into a solid [57,58]. At the same time, lots of contributions have been made to improve the FMT. Kierlik and Rosinberg have proposed a simplified version of FMT, which requires only four scalar weight functions [32]. Roth et al. and Wu et al. have independently, published the white-bear version [60] or the modified FMT [70] using the Mansoori–Carnahan–Starling–Leland bulk equation of state to make simulation results more accurate. For inhomogeneous fluids of nonspherical hard particles, Mecke et al. have derived a fundamental measure theory using the Gauss-Bonnet theorem [22]. In numerical calculation, due to the complexity of FMT, calculations are mostly reduced to 1D cases using geometric symmetry of the simulation systems [22,31,59,60,70]. Only a few literatures provided 3D results [15,16,36,62]. When FMT is combined with the PNP model to include hard sphere repulsion for non-equilibrium transport studies, the final integro-differential equations are more complex and computationally expensive, especially in the situation with biomolecular systems. Liu et al. have made some mathematical analysis on the PNP system for ion flow with density functional theory for hard sphere interaction in 1D situation [28,42]. So far, most studies are restrained to 1D case [19,20,26,28,42]. Recently, Gillespie et al. [34] and Meng et al. [46] have reported simulations of 3D systems. The main difficulty is the calculation of the nonlocal components originated from the Helmholtz free energy.

In this work, we propose a 3D local hard sphere PNP (LHSPNP) model for real biomolecular systems in ionic solutions. On one hand, 3D simulation can count for the irregular boundary of biomolecule which plays an essential role during biological processes, such as ionic flow across channel, protein modification or interaction with a protein or substrate molecule and cell signaling [44,68]. These shape information is hard to be captured in 1D case resulted from the symmetric boundary simplifications. On the other hand, the local hard sphere (LHS) model largely simplifies the numerical calculations while it still partially maintains the effects of hard sphere repulsion.

We improve the PNP model by considering the hard sphere repulsion from FMT. The excess Helmholtz free energy of FMT is employed to generate the excess hard sphere chemical potential which is completely ignored in the PNP model. Different from the ideal chemical potential, this excess component of a certain ion at a given point is determined by an integration about all ion concentrations in a region around the given point, rather than the certain ion concentration at the given point. This integration is in the form of convolution. Gillespie et al. have used fast Fourier transform to deal with the convolution [34], while Meng et al. have used the definition of Dirac delta function and change of variables to transform these 3D integrals into 2D integrals on spheres and remove the singularity in the integrands [46]. Though both algorithms can solve the integro-differential equations, they cost lots of computer memory and time during calculation. We aim to construct an excess chemical potential in a point to point way like the ideal component for 3D simulations of ionic solutions. Liu et al. have derived a LHS excess chemical potential in 1D case and made theoretical analysis on the model problem based on geometric singular perturbation theory [38]. In our work, we concentrate on the more complex 3D case and simplify the integration using an expansion of the integrand under small ionic diameters to obtain the final LHSPNP model. It's found that the 3D LHSPNP model is exactly the same as Liu's when reduced to 1D case.

We examine the effects of the LHS model both from a theoretical and a numerical point of view. For the case of one component homogeneous fluid, the virial coefficients are investigated through the equations of state from the FMT, our local approximation and the size modified model [6,33,43] studied in former work. For FMT, the equation of state is known to be the

Percus-Yevick compressibility equation, equivalent to scaled particle theory, which provides the first three virial coefficients exactly. Frydel and Levin have shown that the size modified model only predicts the first virial coefficient exactly [17]. Based on these discussions and the relations between bulk grand canonical potentials from the micro and macro views, we derive the virial coefficients for our local approximation. We find that the LHS model provides the first two virial coefficients exactly, which performs better than the size modified model. Numerically, to investigate the effects of the hard sphere repulsion from LHS model, we make numerical comparisons for a spherical cavity case among the PNP, LHSPNP, SMPNP models and the Monte Carlo (MC) simulation. For the four parts of the local excess chemical potential in LHSPNP, we notice that the first term is, to some extent, similar to the local excess chemical potential of the SMPNP model, though LHSPNP and SMPNP are based on two different theoretical frameworks. We consider two counterion species in the solution, which helps us to understand competitions between them under the PNP, LHSPNP and SMPNP models. However, in real biomolecular systems, like enzyme molecules and ion channels, the boundary is rarely spherical and may be rather complex. The effects of the boundary shape will be different and may be quite important. The shape of the cavity determines details of confinement (and concentration) of the crowded ions and these in turn determines (for example) the selectivity of calcium channels [3–5,30]. Besides of the complexity of the geometry, it's also necessary to take care of the charge distribution on the biomolecular outer boundary which usually is specific and controls the contents and function of the whole systems, for example, ion channels studied in Refs. [13] and [18]. These should be carefully treated when applied for real biomolecular systems and will be considered explicitly in our future work.

The rest of the paper is organized as follows. The method section offers a detailed description about the derivation of the LHSPNP model, its equation of state in one component uniform fluid, and the numerical method to solve the LHSPNP equations. The result and discussion section provides numerical results of a spherical cavity in various bulk concentrations with the PNP, LHSPNP, SMPNP models and MC simulation and also some discussions about the observed phenomena. Finally, conclusions are summarized in the conclusion section.

2 Method

2.1 Local Hard Sphere Poisson–Nernst–Planck Model

In addition to the ideal chemical potential considered in the original Poisson–Nernst–Planck (PNP) equations, an excess chemical potential arising from hard sphere repulsion is incorporated to the equations to make the model more accurate. Using the constitutive relations about the flux and the electrochemical potential, we have the following expression of ion flux

$$J_i = -m_i c_i \nabla \mu_i = -\frac{D_i}{k_B T} c_i \nabla \mu_i, \tag{1}$$

where J_i is the flux, m_i and c_i are the mobility and concentration for the ith ion species respectively, μ_i is the chemical potential, D_i is the diffusion coefficient, k_B and T are the Boltzmann constant and absolute temperature. The chemical potential μ_i is composed of two parts, the ideal part μ_i^{id} and the excess part μ_i^{ex}. The mass and current conservation law leads to the following equation

$$\frac{\partial c_i}{\partial t} = -\nabla \cdot J_i = \nabla \cdot \left(\frac{D_i}{k_B T} c_i \nabla \mu_i \right) = \nabla \cdot \left(\beta D_i c_i \left(\nabla \mu_i^{id} + \nabla \mu_i^{ex} \right) \right), \qquad (2)$$

where $\mu_i^{id} = q_i \phi + \beta^{-1} \ln \Lambda_i^3 c_i$, ϕ is the electrostatic potential, $\beta = \frac{1}{k_B T}$, q_i and Λ_i are the charge amount and de Broglie wave length of the ith ion species respectively. Coupling Eq. 2 with the Poisson equation, we obtain the modified PNP at steady state

$$\nabla \cdot D_i (\nabla c_i + \beta q_i c_i \nabla \phi + \beta c_i \nabla \mu_i^{ex}) = 0, \quad i = 1, \cdots, K, \qquad (3)$$

$$-\nabla \cdot \epsilon \nabla \phi - \sum_{i=1}^{K} c_i q_i = \sum_{i=1}^{N} Q_i \delta_i, \qquad (4)$$

where K is the number of ion species, and Q_i is the charge amount of the ith atom in the biomolecule that contains N fixed point charges. Specifically, it is worth noting that in equilibrium state of zero flux, the above modified PNP equations become a modified PB model as described by the following equation:

$$-\nabla \cdot \epsilon(\mathbf{x}) \nabla \phi(\mathbf{x}) - \sum_{i=1}^{K} c_{bi} q_i e^{-\beta q_i \phi(\mathbf{x}) - \beta \left(\mu_i^{ex}(\mathbf{x}) - \mu_{bi}^{ex} \right)} = \sum_{i=1}^{N} Q_i \delta_i(\mathbf{x}), \qquad (5)$$

where μ_{bi}^{ex} is the bulk excess chemical potential defined under bulk concentrations. This generalized PB equation incorporating the hard sphere repulsion can be solved by combining with the following local expression of $\mu_i^{ex}(\mathbf{x})$ from FMT.

According to Rosenfeld's fundamental measure theory (FMT) [51], the excess Helmholtz free energy due to hard sphere repulsion can be expressed as

$$\mathscr{F}_{ex}\Big[\{c_i(\mathbf{x})\}\Big] = \beta^{-1} \int d\mathbf{x} \, \Phi\Big[\{n_\alpha(\mathbf{x})\}\Big], \qquad (6)$$

$$\Phi\Big[\{n_\alpha(\mathbf{x})\}\Big] = -n_0 \ln(1 - n_3) + \frac{1}{1 - n_3}(n_1 n_2 - n_{V1} \cdot n_{V2})$$

$$+ \frac{n_2}{24\pi(1 - n_3)^2}(n_2^2 - 3 n_{V2} \cdot n_{V2}), \qquad (7)$$

$$n_\alpha(\mathbf{x}) = \sum_i \int c_i(\mathbf{x}') \omega_i^{(\alpha)}(\mathbf{x} - \mathbf{x}') d\mathbf{x}', \qquad (8)$$

where $n_\alpha(\mathbf{x})$ is the weighted density, $\omega_i^{(\alpha)}(\mathbf{x})$ is the characteristic (weight) function for $\alpha = 0, 1, 2, 3, V1, V2$. The indexes $V1$ and $V2$ are used to represent the vector terms while the other four represent the scalar terms. For a three-dimensional hard sphere particle of radius R_i, these functions are defined as:

$$\omega_i^{(3)}(\mathbf{x}) = \theta(|\mathbf{x}| - R_i), \qquad (9)$$

$$\omega_i^{(2)}(\mathbf{x}) = \delta(|\mathbf{x}| - R_i), \qquad (10)$$

$$\omega_i^{(1)}(\mathbf{x}) = \omega_i^{(2)}(\mathbf{x})/4\pi R_i, \qquad (11)$$

$$\omega_i^{(0)}(\mathbf{x}) = \omega_i^{(2)}(\mathbf{x})/4\pi R_i^2, \qquad (12)$$

$$\omega_i^{(V2)}(\mathbf{x}) = \frac{\mathbf{x}}{|\mathbf{x}|} \delta(|\mathbf{x}| - R_i), \qquad (13)$$

$$\omega_i^{(V1)}(\mathbf{x}) = \omega_i^{(V2)}(\mathbf{x})/4\pi R_i. \qquad (14)$$

$\theta(x)$ is the unit step function defined by

$$\theta(x) = \begin{cases} 0 \text{ if } x > 0, \\ 1 \text{ if } x \leq 0, \end{cases} \tag{15}$$

and $\delta(x)$ is the Dirac delta function.

From above definitions, it's not difficult to obtain the following expression of the excess chemical potential

$$\mu_i^{ex}(x) = \frac{\delta \mathscr{F}_{ex}}{\delta c_i} = \beta^{-1} \int dx' \sum_\alpha \frac{\partial \Phi}{\partial n_\alpha} \Big[\{n_\gamma(x)\} \Big] \omega_i^{(\alpha)}(x' - x), \tag{16}$$

where

$$\frac{\partial \Phi}{\partial n_0} = -\ln(1 - n_3), \tag{17}$$

$$\frac{\partial \Phi}{\partial n_1} = \frac{n_2}{1 - n_3}, \tag{18}$$

$$\frac{\partial \Phi}{\partial n_2} = \frac{n_1}{1 - n_3} + \frac{1}{8\pi(1 - n_3)^2}(n_2^2 - n_{V2} \cdot n_{V2}), \tag{19}$$

$$\frac{\partial \Phi}{\partial n_3} = \frac{n_0}{1 - n_3} + \frac{1}{(1 - n_3)^2}(n_1 n_2 - n_{V1} \cdot n_{V2}) + \frac{n_2}{12\pi(1 - n_3)^3}$$
$$\times (n_2^2 - 3 n_{V2} \cdot n_{V2}), \tag{20}$$

$$\frac{\partial \Phi}{\partial n_{V1}} = -\frac{n_{V2}}{1 - n_3}, \tag{21}$$

$$\frac{\partial \Phi}{\partial n_{V2}} = -\frac{n_{V1}}{1 - n_3} - \frac{1}{4\pi} \frac{n_2 n_{V2}}{(1 - n_3)^2}. \tag{22}$$

As shown in Eq. 16, the excess chemical potential resulted from hard sphere repulsion is an integration defined on a certain region, which requires plenty of calculation. By taking corresponding Taylor expansions of the excess chemical potential, we can deduce a local formula for the excess chemical potential as follows. From Eq. 16, the excess chemical potential of the ith ion species can be decomposed into six components. Denote them by $\{\mu_i^\alpha(x) = \beta^{-1} \int \frac{\partial \Phi}{\partial n_\alpha} [\{n_\gamma(x)\}] \omega_i^{(\alpha)}(x' - x) dx'\}$ and we can get:

$$\beta \mu_i^0(x) = -\ln\left(1 - \sum_j \frac{4}{3}\pi R_j^3 c_j(x)\right) + O(R^4), \tag{23}$$

$$\beta \mu_i^1(x) = \frac{R_i \sum_j 4\pi R_j^2 c_j(x)}{1 - \sum_j \frac{4}{3}\pi R_j^3 c_j(x)} + O(R^4), \tag{24}$$

$$\beta \mu_i^2(x) = \frac{4\pi R_i^2 \sum_j R_j c_j(x)}{1 - \sum_j \frac{4}{3}\pi R_j^3 c_j(x)} + O(R^4), \tag{25}$$

$$\beta \mu_i^3(x) = \frac{4}{3}\pi \frac{R_i^3 \sum_j c_j(x)}{1 - \sum_j \frac{4}{3}\pi R_j^3 c_j(x)} + O(R^4), \tag{26}$$

$$\beta \mu_i^{V1}(x) = O(R^4), \tag{27}$$

$$\beta \mu_i^{V2}(x) = O(R^4). \tag{28}$$

Here, we give the explicit derivation of Eq. 23 as an example. Others can be obtained in the similar way. First, consider the expansion of $n_3(x)$ in the definition of $\beta\mu_i^0(x)$:

$$
\begin{aligned}
n_3(x) &= \sum_i \int c_i(x')\omega_i^{(3)}(x-x')dx' = \sum_i \int c_i(x-x')\omega_i^{(3)}(x')dx' \\
&= \sum_i \int_{|x'|\le R_i} c_i(x-x')dx' \\
&= \sum_i \int_{|x'|\le R_i} \left[c_i(x) - \nabla c_i(x)\cdot x' + O(R^2) \right] dx' \\
&= \sum_i \frac{4}{3}\pi R_i^3 c_i(x) + O(R^5).
\end{aligned}
\tag{29}
$$

Then, substituting above equation for $n_3(x)$ in the expansion of $\beta\mu_i^0(x)$, we have:

$$
\begin{aligned}
\beta\mu_i^0(x) &= \int \frac{\partial\Phi}{\partial n_0}(x')\omega_i^{(0)}(x-x')dx' = \int \frac{\partial\Phi}{\partial n_0}(x-x')\omega_i^{(0)}(x')dx' \\
&= -\int \ln\left(1 - n_3(x-x')\right)\frac{1}{4\pi R_i^2}\delta(|x'|-R_i)dx' \\
&= -\int_0^{2\pi} d\phi \int_0^\pi \sin\theta d\theta \int_0^\infty \ln\left(1 - n_3(x-rv)\right)\frac{r^2}{4\pi R_i^2}\delta(r-R_i)dr \\
&= -\frac{1}{4\pi}\int_0^{2\pi} d\phi \int_0^\pi \ln\left(1 - n_3(x-R_i v)\right)\sin\theta d\theta \\
&= -\frac{1}{4\pi}\int_0^{2\pi} d\phi \int_0^\pi \left[\ln\left(1 - n_3(x)\right) \right. \\
&\qquad \left. + \frac{-\nabla n_3(x)}{1-n_3(x)}\cdot(-R_i v) + O(\|\nabla^2 n_3(x)\|R^2) \right]\sin\theta d\theta \\
&= -\ln\left(1 - n_3(x)\right) + O(R^4) \\
&= -\ln\left(1 - \sum_j \frac{4}{3}\pi R_j^3 c_j(x) + O(R^5)\right) + O(R^4) \\
&\approx -\ln\left(1 - \sum_j \frac{4}{3}\pi R_j^3 c_j(x)\right) + O(R^4),
\end{aligned}
\tag{30}
$$

The other terms can be obtained similarly, as shown in Eqs. 24–28. Take the lowest order approximation of each term and the local excess chemical potential in three dimensions is given by:

$$
\begin{aligned}
\beta\mu_i^{LHS}(x) &= \beta\sum_\alpha \mu_i^\alpha(x) \\
&= -\ln\left(1 - \sum_j \frac{4}{3}\pi R_j^3 c_j(x)\right) + \frac{R_i\sum_j 4\pi R_j^2 c_j(x)}{1-\sum_j \frac{4}{3}\pi R_j^3 c_j(x)} \\
&\quad + \frac{4\pi R_i^2 \sum_j R_j c_j(x)}{1-\sum_j \frac{4}{3}\pi R_j^3 c_j(x)} + \frac{4}{3}\pi\frac{R_i^3\sum_j c_j(x)}{1-\sum_j \frac{4}{3}\pi R_j^3 c_j(x)}.
\end{aligned}
\tag{31}
$$

It's notable that the excess chemical potential expressed by Eq. 31 at a given point is determined by the concentration values at this point. This local expression is much simpler than the nonlocal one in numerical calculation. For one dimensional situation, a local hard sphere potential is also proposed by Liu et al. [38] to investigate ion flow through channels and shows great improvements.

The final modified Nernst–Planck (NP) equations of the local hard sphere PNP (LHSPNP) can be obtained by replacing the μ_i^{ex} in Eq. 3 by $\mu_i^{LHS}(\boldsymbol{x})$ in Eq. 31

$$\nabla \cdot D_i(\boldsymbol{x})\Big(\nabla c_i(\boldsymbol{x}) + \beta q_i c_i(\boldsymbol{x})\nabla\phi(\boldsymbol{x}) + \beta c_i(\boldsymbol{x})\nabla\mu_i^{LHS}(\boldsymbol{x})\Big) = 0, \quad i = 1, \cdots, K. \quad (32)$$

In the size modified PNP (SMPNP) equations proposed in our former work [43,50], the excess chemical potential is expressed by $\mu_i^{ex}(\boldsymbol{x}) = -\beta^{-1}k_i \ln\left(1 - \sum_j a_j^3 c_j(\boldsymbol{x})\right)$, where $k_i = \frac{a_i^3}{a_0^3}$, a_i and a_0 are the diameters of ion and water molecule, respectively. This is quite similar to the first term of the local hard sphere excess chemical potential $\mu_i^{LHS}(\boldsymbol{x})$ in Eq. 31. From this point of view, the LHSPNP can capture the same ionic size effects contained in the SMPNP model. Furthermore, it's found that all the four terms of Eq. 31 are positive and contribute unfavorable energies for all possible concentrations, which indicates the later three terms have the similar influence as the first term and strengthen the hard sphere repulsion effect. Compared with the excess chemical potential in SMPNP model, these extra three terms in $\mu_i^{LHS}(\boldsymbol{x})$ can be regarded as supplements to the size effects.

2.2 Bulk Fluid Equation of State

In uniform fluid with constant density, the equation of state for FMT is known to be the Percus-Yevick compressibility equation, which is the same as the scaled particle theory [14,51,60]. The four scalar weighted densities $\{n_\alpha\}(\alpha = 0, 1, 2, 3)$ can be reduced to $\{\xi^{(\alpha)}\}$ where $\xi^{(3)} = \frac{4\pi}{3}\sum_i c_i R_i^3$, $\xi^{(2)} = 4\pi \sum_i c_i R_i^2$, $\xi^{(1)} = \sum_i c_i R_i$ and $\xi^{(0)} = \sum_i c_i$, while the vector weighted densities n_{V1} and n_{V2} vanish. The bulk grand canonical potential is given by

$$\Omega_b = \left(\beta^{-1}\Phi_b + f_b^{id} - \sum_i \mu_i c_i\right)V, \quad (33)$$

where $\beta^{-1}\Phi_b$ is the bulk excess energy density defined in Eq. 7, f_b^{id} is the bulk ideal energy density defined by $\beta^{-1}\sum_i c_i(\ln c_i \Lambda_i^3 - 1)$ and V is the system volume [14]. On the other hand, Ω_b can also be determined from the thermodynamic relation

$$\Omega_b = -PV, \quad (34)$$

where P is the pressure [14]. From Eqs. 33 and 34, the pressure is expressed as:

$$P = \sum_i \mu_i c_i - \beta^{-1}\Phi_b - f_b^{id}. \quad (35)$$

According to the equilibrium condition, the chemical potential μ_i at bulk state is $\frac{\partial f}{\partial c_i}$, where f is the energy density composed of the excess and ideal parts in the FMT. This leads to the general expression of pressure in the following equation:

$$P = \sum_i c_i \frac{\partial f}{\partial c_i} - f. \quad (36)$$

In studying the equation of state, we consider one component bulk fluid with constant density ρ. Under this assumption, the bulk excess energy density from Eq. 7 is

$$\Phi_b = -\rho \ln(1-\eta) + \frac{3\eta\rho}{1-\eta} + \frac{3\eta^2\rho}{2(1-\eta)^2}, \tag{37}$$

where η is the packing fraction defined by $\eta = \frac{\pi\sigma^3}{6}$ and σ is the diameter of ions in solution. Thus we can get the energy density, and the equation of state

$$\frac{\beta P}{\rho} = \frac{1+\eta+\eta^2}{(1-\eta)^3} = 1 + \sum_{i=1}^{\infty} \frac{3i^2+3i+2}{2}\eta^i = 1 + 4\eta + 10\eta^2 + 19\eta^3 + \cdots. \tag{38}$$

Based on tabulated values of the first eight virial coefficients [21], the equation of state for homogeneous hard sphere fluid is given by

$$\frac{\beta P}{\rho} = 1 + 4\eta + 10\eta^2 + 18.365\eta^3 + 28.225\eta^4 + 39.74\eta^5 + 53.5\eta^6 + 70.8\eta^7 + \cdots \tag{39}$$

It's apparent that the first three virial coefficients are exact from FMT in Eq. 38.

In our local hard sphere approximation, we replace the weighted densities with a local expression by ignoring the Taylor expansion terms of order $O(\sigma^m)(m \geqslant 4)$, and use it in the derivation of excess chemical potentials. With this consideration, the bulk excess energy density in local hard sphere model is given by

$$\Phi_b^{LHS} = -\rho \ln(1-\eta) + \frac{3\eta\rho}{1-\eta}. \tag{40}$$

Compared with Eq. 37, this equation does not take into account the last term of order $O(\eta^2) = O(\sigma^6)$. Following this definition, we can get the bulk excess chemical potential after ignoring the terms of order $O(\sigma^m)(m \geqslant 4)$

$$\beta\mu_b^{ex} = \frac{\partial \Phi_b^{LHS}}{\partial \rho} = -\ln(1-\eta) + \frac{7\eta}{1-\eta}. \tag{41}$$

This is in accordance with our above result of Eq. 31 in one component bulk condition. Substituting these expressions of excess energy density and chemical potential, and those of the ideal parts into Eq. 36, we finally get

$$\frac{\beta P}{\rho} = \frac{1+3\eta}{1-\eta} = 1 + 4\sum_{i=1}^{\infty} \eta^i = 1 + 4\eta + 4\eta^2 + \cdots. \tag{42}$$

It's clear the first two virial coefficients from Eq. 42 is exact, which is reasonable with the approximation that we do not take into account the terms of order $O(\eta^n)(n \geqslant 2)$. For the later terms in the order of $O(\eta^n)(n \geqslant 2) = O(\sigma^m)(m \geqslant 6)$ in Eq. 42, they can not be predicted well in LHS, since the terms of order $O(\sigma^m)(m \geqslant 6)$ are ignored.

For the size modified model [6,33,43] with one component bulk fluid, Frydel and Levin have arrived at the following conclusion [17]

$$\frac{\beta P}{\rho} = -\frac{1}{\eta} \ln(1-\eta) = 1 + \sum_{i=1}^{\infty} \frac{1}{i+1}\eta^i = 1 + \frac{1}{2}\eta + \cdots. \tag{43}$$

Different from the FMT and LHS predictions, above equation only provides the first virial coefficient accurately. Figure 1 illustrates the compressibility factor $Z = \frac{\beta P}{\rho}$ versus packing fraction η of the three different results discussed in Eqs. 38, 42 and 43. From the inset of

Fig. 1 (Color online) The equation of state of pure hard sphere fluid
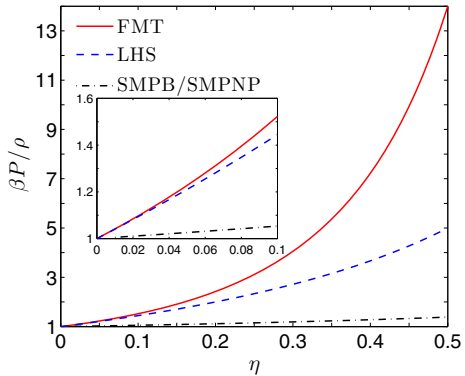
Fig. 1, it's notable that at low η values, the predictions between FMT and our local approach are quite close to each other, while the values from the size modified models SMPB/SMPNP [6,33,43] are much lower than those from FMT and LHS.

2.3 Numerical Method

Finite element method (FEM) is employed in our work to solve the three different models, PNP, SMPNP and LHSPNP, numerically. To accelerate the calculations, the algorithms are implemented with the parallel adaptive finite element package PHG [71]. The molecular surface and volume meshes, that are necessary for FEM computation, are generated by TMSmesh [10,11] and Tetgen [63].

Similar to our former work [43], using Slotboom transformation, the modified NP equation Eq. 32 can be written in a symmetric form

$$\nabla \cdot (\bar{D}_i \nabla \bar{c}_i) = 0, \tag{44}$$

where $\bar{D}_i = D_i e^{-V_i}$, $\bar{c}_i = c_i e^{V_i}$ and $V_i = \beta q_i \phi + \beta \sum_\alpha \mu_i^\alpha$. Substituting the above transformed concentration into Poisson equation, we have

$$-\nabla \cdot \epsilon \nabla \phi - \sum_{i=1}^{K} \bar{c}_i e^{-V_i} q_i = \sum_{i=1}^{N} Q_i \delta_i. \tag{45}$$

It's notable that the weak form of Eq. 44 is symmetric and linear in finite element method, and Eq. 45 leads to a nonlinear weak form. Similar weak forms and the bilinear forms for FEM to solve the SMPNP have been presented explicitly in our former work [68,69]. To deal with the nonlinearity of the weak form of Eq. 45, we use Newton method to linearize the system as given in previous work [68,69]. Also, relaxation iteration is employed to obtain convergent simulation results for the coupled PDE systems.

3 Result and Discussion

In this section, a spherical cavity of radius $10\,\text{Å}$ in ionic solution is taken as a simulation example. The total computational region is a sphere of radius $80\,\text{Å}$ which has the same origin as the spherical cavity. Numerical tests are first performed in a 1:1 electrolyte solution, in which K^+ and Cl^- are added, to study the influence of ionic size effects in various conditions
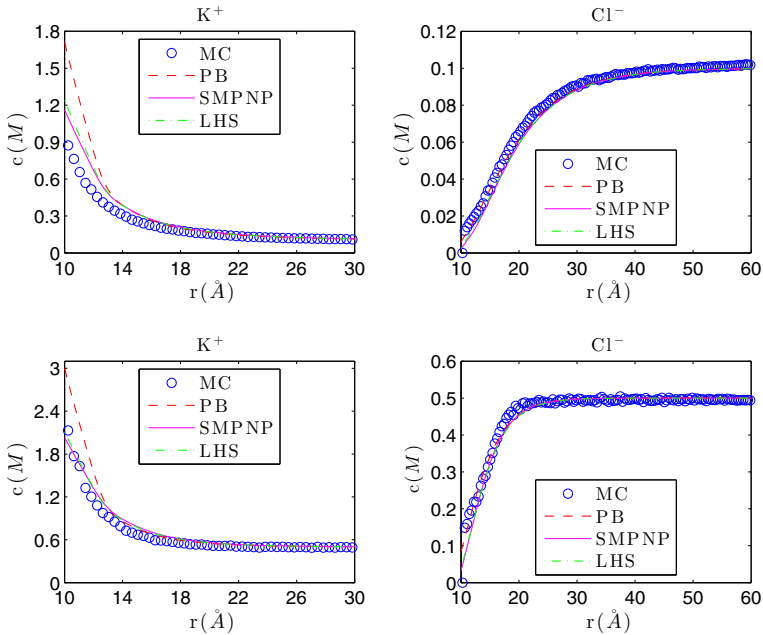
Fig. 2 (Color online) Concentrations of K^+ and Cl^- at two different bulk concentrations: (1) $c_b = 0.1\,M$ (*upper panel*) and (2) $c_b = 0.5\,M$ (*lower panel*) when the central charge of spherical cavity Q is $-10e_c$

by comparisons among the LHSPNP, SMPNP, PB models and the MC simulation. It's notable that the PB description for continuum model is equivalent to the steady state PNP equations at equilibrium state [45]. The diameters of these two ion species required in LHSPNP, SMPNP and MC calculations are: $a(K^+) = 5.51\,\text{Å}$ and $a(Cl^-) = 6.37\,\text{Å}$ [37]. These values are larger than pure ionic diameters because a hydration shell is considered around ions in solution. Figures 2 and 3 illustrate the density profiles when bulk concentrations are 0.1 M (upper panels) and 0.5M (lower panels). It is worth noting that because of volume exclusion, the ion density in MC simulation vanishes in the region within an ion radius to the cavity surface. To make a clearer comparison, the curves from MC data in both figures are shifted half the ion diameters towards the origin. As shown in the upper panel of Fig. 2 at low bulk concentration and low central charge, the simulation results among the four methods are close to each other and the difference between the SMPNP and LHSPNP model is small. However, when the central charge increases to $-40e_c$ shown in Fig. 3, the concentration of K^+ from the MC simulation is considerably larger than those from the SMPNP and LHSPNP calculations. This seems that the SMPNP and LHSPNP models overestimate the volume exclusion effects in the environment of strong electric field and condensed ionic density. While in MC simulation, the ion correlation effects that are missed in SMPNP and LHSPNP can enhance the condensation of counter ions in the situation. As shown in both Figs. 2 and 3, the LHSPNP tends to result in a slightly higher counter ion concentration near the sphere than the SMPNP model.

In order to investigate the competition among various kinds of counterions, two positive ion species, K^+ and Ca^{2+}, and one negative ion species, Cl^- are added in the solution. The neutrality condition is applied on the boundary of the computational region. In the following, if not specified, the bulk concentration of K^+ is set to be $c_{b1} = 0.1\,M$. Only the bulk concentration of Ca^{2+}, c_{b2} is varied. The bulk concentration of Cl^-, c_{b3} is then determined
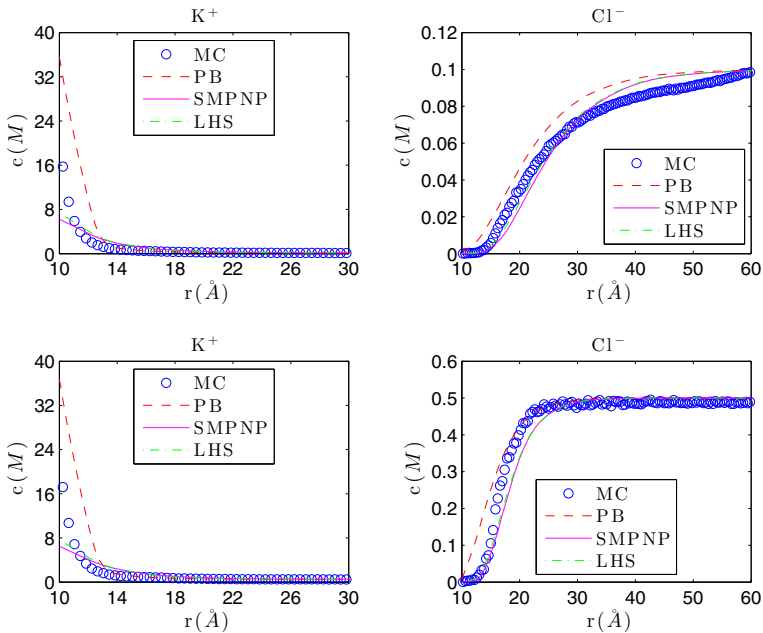
Fig. 3 (Color online) Same as in Fig. 2 but for $Q = -40e_c$

from the neutrality condition. Three models, LHSPNP, SMPNP and PB models are used to simulate the spherical cavity in ionic solution, respectively. The concentration profiles of different ion species in the steady state are obtained from the numerical solutions of those models for comparison. The spherical cavity contains a central charge of $-40e_c$ and the diameter of Ca^{2+} is 4.75 Å [37]. In the figures below, solid curve is applied for K^+, and dashed curve for Ca^{2+}.

Figure 4 shows the concentration profiles of Ca^{2+} obtained from the three models at two different bulk values. In Fig. 4a, when the bulk concentration of Ca^{2+} is 10^{-3} M, the PB predictions overestimate the concentrations compared with those of SMPNP and LHSPNP. And the concentration from PB decreases quickly to smaller values than the other two predictions in a narrow region within a distance of 0.4 Å to the cavity surface. However, when $c_{b2} = 10^{-4}$ M, the SMPNP and LHS predictions are always higher than the PB, even near the spherical surface. This indicates PB model can also lead to underestimation of concentration for counterions when its bulk concentration is small enough. This may be explained as follows. According to the Boltzmann distribution, the following equations hold:

$$c(K^+) = c_{b1}e^{-e_c\beta\phi}, \quad c(Ca^{2+}) = c_{b2}e^{-2e_c\beta\phi}, \tag{46}$$

$$\frac{c(K^+)}{c(Ca^{2+})} = \frac{c_{b1}}{c_{b2}}e^{e_c\beta\phi}. \tag{47}$$

Equation 47 can be reduced to $\frac{c(K^+)}{c(Ca^{2+})} = 10^3 e^{e_c\beta\phi}$, when c_{b1} and c_{b2} are 0.1 and 10^{-4} M, respectively. The reduced potential $u = e_c\beta\phi$ is about -6 under the given neutrality boundary conditions, resulting in the ratio $\frac{c(K^+)}{c(Ca^{2+})}$ larger than 2. Therefore, K^+ plays a leading role in neutralizing the fixed negative charge, while the concentration of Ca^{2+} may be underestimated by the PB model. Besides, it's easy to see that in both subfigures of Fig. 4 the predictions from
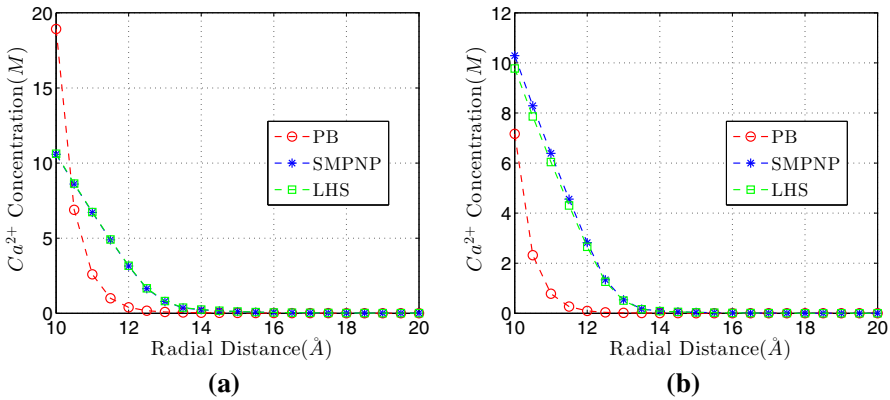
Fig. 4 (Color online) Concentrations of Ca^{2+} at two different bulk concentrations: **a** $c_{b2} = 10^{-3}$ M and **b** $c_{b2} = 10^{-4}$ M
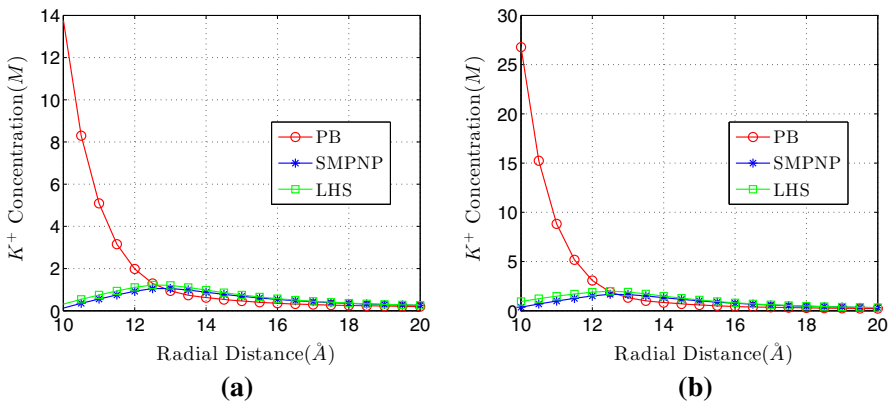
Fig. 5 (Color online) Concentrations of K^+ at two different bulk concentrations: **a** $c_{b2} = 10^{-3}$ M and **b** $c_{b2} = 10^{-4}$ M

PB model decrease faster than the others, which can be explained by Eq. 46. This heavily exponential decrease is resulted from the quick enhancement of the reduced potential u in the vicinity of the spherical cavity.

Figure 5 presents the predictions of K^+ at the same bulk values mentioned above for Fig. 4. According to the neutrality boundary condition, the c_{b3} values are then 0.102 and 0.1002 M, respectively. As is known, the counterion concentration predicted from the traditional PB model is unphysically high in the vicinity of the biomolecule [6,50]. This is clearly shown in the two subfigures of Fig. 5. The concentration on the spherical surface can reach as high as 13.5 M when $c_{b2} = 10^{-3}$ M. As the radial distance increases, the concentration decreases to the bulk value quickly. For SMPNP and LHSPNP models, a stratification of K^+ is observed, which is quite different from the monotonic phenomenon of the PB model. With the increasing of the radial distance, the concentration first increases to a highest value then decreases to the bulk value slowly. In SMPNP, ionic size effects are incorporated through adding an additional entropy term to the free energy, leading to an extra excess chemical potential. In LHSPNP, hard sphere repulsion described by the FMT is added to the free energy and then the excess
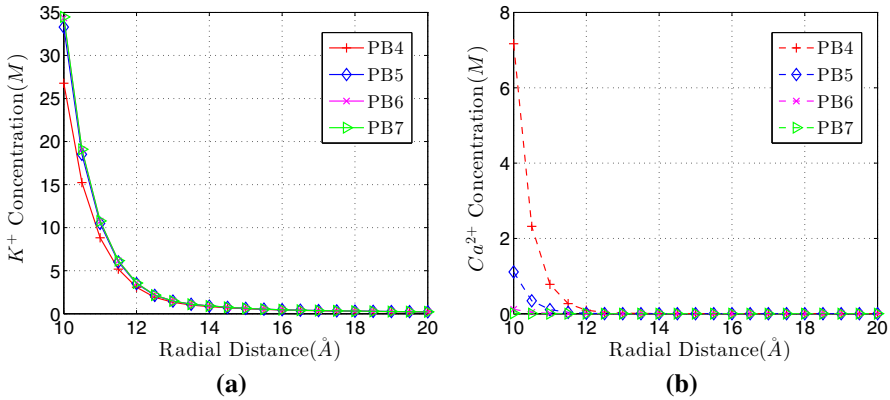
Fig. 6 (Color online) Concentrations of two ion species: **a** K^+ and **b** Ca^{2+} calculated from the original PB model. Four different bulk concentrations are considered: (1) PB4: $c_{b2} = 10^{-4}$ M, (2) PB5: $c_{b2} = 10^{-5}$ M, (3) PB6: $c_{b2} = 10^{-6}$ M and (4) PB7: $c_{b2} = 10^{-7}$ M

chemical potential is approximated locally. Both models can capture the stratification of K^+ through adding extra terms to the chemical potential. This change originates from the reasonable assumption that ions in solution are regarded as finite volumes rather than point charges. Since Ca^{2+} carries one more positive elementary charge than K^+, huge accumulation of Ca^{2+} around the charged spherical cavity prevents the enhancement of K^+. Nevertheless, as the radial distance becomes larger, the electric field strength becomes smaller and so does the concentration of Ca^{2+}. Thus the repelling from the Ca^{2+} weakens and the concentration of K^+ increases to a certain value in a finite distance. At further distance, the weakening of electric field makes the concentration of K^+ decrease. This explains the stratification of K^+ from results of SMPNP and LHSPNP models.

Next, we vary the c_{b2} value from 10^{-4} M to 10^{-7} M in which the ratio of $\frac{c_{b1}}{c_{b2}}$ can reach as high as 10^6, while the other conditions remain the same as aforementioned. Under these circumstances, Figs. 6, 7, 8 illustrate the concentration profiles of the two positive ion species resulted from the PB, SMPNP and LHSPNP models. In Fig. 6, it's observed that both positive ion concentrations decrease as the radial distance increases and that the concentration of K^+ is larger than that of Ca^{2+} under same conditions. These phenomena can be explained by the Boltzmann concentrations defined in Eqs. 46 and 47. Similar explanations have been presented in above analysis for Figs. 4 and 5. In addition, with the decrease of the c_{b2}, the enhancement of $c(K^+)$ is clear (Fig. 6a), while $c(Ca^{2+})$ decreases accordingly (Fig. 6b). This also occurs in the SMPNP and LHSPNP models as shown in Figs. 7 and 8.

In Figs. 7a and 8a, the stratification of K^+ disappears when the bulk concentration of Ca^{2+} is smaller than 10^{-5} M. This is a straightforward result from the decrease of c_{b2}. Though Ca^{2+} ions are much easier to be attracted to the spherical surface than K^+, the number of Ca^{2+} is so tiny that they have no significant influence on the accumulation of K^+. Therefore, a great number of K^+ can be attracted to the neighborhood of the spherical surface. As the radial distance increases, the concentration of K^+ decreases gradually to the bulk values attributed to the weakening of the electric potential. In contrast to the stratification of K^+ appeared at certain cases, the concentration of Ca^{2+} always decreases monotonically with the increasing of the radial distance, even when its bulk value is 10^{-7} M. This means the bulk concentration is not the essential factor for ion stratification. For SMPNP at given conditions, Li et al. have shown that the phenomenon depends on the ratio of ionic charge amount over its volume [37].
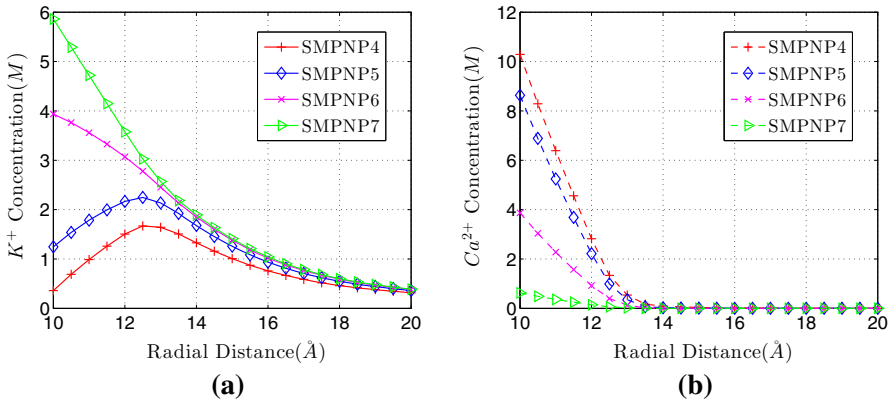
Fig. 7 (Color online) Concentrations of two ion species: **a** K^+ and **b** Ca^{2+} when ionic size effects are incorporated. Four different bulk concentrations are considered: (1) SMPNP4: $c_{b2} = 10^{-4}$ M, (2) SMPNP5: $c_{b2} = 10^{-5}$ M, (3) SMPNP6: $c_{b2} = 10^{-6}$ M and (4) SMPNP7: $c_{b2} = 10^{-7}$ M
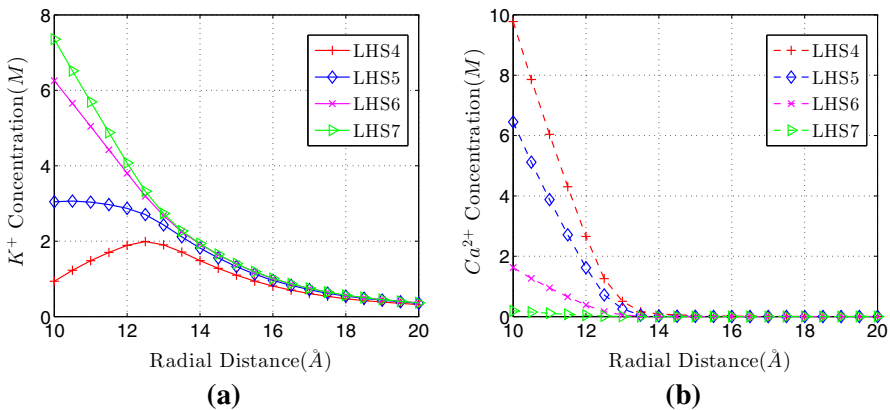
Fig. 8 (Color online) Concentrations of two ion species: **a** K^+ and **b** Ca^{2+} when local hard sphere excess chemical potential is included. Four different bulk concentrations are considered: (1) LHS4: $c_{b2} = 10^{-4}$ M, (2) LHS5: $c_{b2} = 10^{-5}$ M, (3) LHS6: $c_{b2} = 10^{-6}$ M and (4) LHS7: $c_{b2} = 10^{-7}$ M

For the similar spherical case with mixed ion species, the concentration of the ion with the largest or the smallest ratio changes monotonically as the radial distance increases, while the other ion species' concentrations may appear with stratification phenomenon. In our settings, the following relation holds:

$$\frac{q(Ca^{2+})}{a^3(Ca^{2+})} > \frac{q(K^+)}{a^3(K^+)} > \frac{q(Cl^-)}{a^3(Cl^-)}. \tag{48}$$

As a result, the change of Ca^{2+} is always monotonic, while the stratification occurs only for K^+. In Fig. 8, the numerical results from LHS models also show these properties.

However, difference between the SMPNP and the LHSPNP models is also observed in Figs. 7 and 8. When $c_{b2} = 10^{-5}$ M, the stratification of K^+ occurs in the SMPNP model but not in the LHSPNP model. Furthermore, there is also a small difference between Ca^{2+} concentration profiles from SMPNP (Fig. 7b) and LHSPNP (Fig. 8b) models. The Ca^{2+}

concentration from LHSPNP simulations is smaller than that from SMPNP under the same boundary conditions. This indicates that the LHSPNP model captures more about the exclusion effects of Ca^{2+} than the SMPNP model. In SMPNP, when the bulk concentration c_{b2} is 10^{-5} M, Ca^{2+} is still much easier to be attracted than K^+. But for LHSPNP model, the number of Ca^{2+} is not enough to prevent K^+ from accumulation around the sphere. Therefore, in LHSPNP, the stratification of K^+ does not happen under this condition. When c_{b2} is 10^{-6} M or less, no stratification occurs in either SMPNP or LHSPNP modeling.

4 Conclusion

We have proposed a local hard sphere PNP model to account for hard sphere repulsion in three dimensional ionic solutions. Compared with the PNP model, the LHSPNP model contains an extra local excess chemical potential, derived from the expansion of the variation of the excess Helmholtz free energy (excess chemical potential) from FMT. This local expression avoids solving of integro-differential equations which requires much more computer memory and time. It is interesting to notice that one component of our local excess chemical potential is similar to the key part in SMPNP model. This indicates that in some sense, the LHSPNP model essentially contains the previous SMPB/SMPNP models [6,33,43], though these two models are from different backgrounds. The closeness between these two models under certain conditions are also demonstrated by numerical computations in this work.

Theoretical study on the equation of state of one component homogeneous fluid shows that the LHS model can predict exactly the first two virial coefficients, performing better than the size modified model which only provides the first coefficient accurately. Numerical tests for an example of a spherical cavity in ionic solutions indicate the LHSPNP model can avoid unphysical accumulation of counterions around biomolecular surface. But when the bulk concentration and the potential are high, the concentration results from LHSPNP model are lower than those from the MC simulation. Under certain bulk concentrations in mixed ionic solution, we find that the concentration of one counterion species in LHSPNP equilibrium simulation is higher than that in PNP simulation. Furthermore, the stratification of counterion is observed when two different counterion species are included in the solution system. These phenomena from LHSPNP model are quite similar to those from SMPNP.

References

1. Abaid, N., Eisenberg, R.S., Liu, W.: Asymptotic expansions of I–V relations via a Poisson–Nernst–Planck system. SIAM. J. Appl. Dyn. Syst. **7**, 1507–1526 (2008)
2. Bazant, M.Z., Kilic, M.S., Storey, B.D., Ajdari, A.: Towards an understanding of induced-charge electrokinetics at large applied voltages in concentrated solutions. Adv. Colloid Interface Sci. **152**, 48–88 (2009)
3. Boda, D., Nonner, W., Valisk, M., Henderson, D., Eisenberg, B., Gillespie, D.: Steric selectivity in Na channels arising from protein polarization and mobile side chains. Biophys. J. **93**, 1960–1980 (2007)
4. Boda, D., Nonner, W., Henderson, D., Eisenberg, B., Gillespie, D.: Volume exclusion in calcium selective channels. Biophys. J. **94**, 3486–3496 (2008)

5. Boda, D., Valisk, M., Henderson, D., Eisenberg, B., Gillespie, D., Nonner, W.: Ionic selectivity in L-type calcium channels by electrostatics and hard-core repulsion. J. Gen. Physiol. **133**, 497–509 (2009)

6. Borukhov, I., Andelman, D., Orland, H.: Steric effects in electrolyte: a modified Poisson–Boltzmann equation. Phys. Rev. Lett. **79**, 435–438 (1997)

7. Borukhov, I., Andelman, D., Orland, H.: Adsorption of large ions from an electrolyte solution: a modified Poisson–Boltzmann equation. Electrochim. Acta **46**, 221–229 (2000)

8. Cahn, J.W., Hilliard, J.E.: Free energy of a nonuniform system I: interfacial free energy. J. Chem. Phys. **28**, 258–267 (1958)

9. Chen, D., Lear, J., Eisenberg, B.: Permeation through an open channel: Poisson–Nernst–Planck theory of a synthetic ionic channel. Biophys. J. **72**, 97–116 (1997)

10. Chen, M., Lu, B.: Tmsmesh: a robust method for molecular surface mesh generation using a trace technique. J. Chem. Theory Comput. **7**, 203–212 (2011)

11. Chen, M., Tu, B., Lu, B.: Triangulated manifold meshing method preserving molecular surface topology. J. Mol. Graph. Model. **38**, 411–418 (2012)

12. Chu, V.B., Bai, Y., Lipfert, J., Herschlag, D., Doniach, S.: Evaluation of ion binding to DNA duplexes using a size-modified Poisson–Boltzmann theory. Biophys. J. **93**, 3202–3209 (2007)

13. Eisenberg, B.: Crowded charges in ion channels. In: Advances in Chemical Physics, pp. 77–223, Wiley, New York (2011)

14. Evans, R.: Density functional theory for inhomogeneous fluids I: Simple fluids in equilibrium. Lectures at 3rd Warsaw School of Statistical Physics, Kazimierz Dolny 27 (2009)

15. Frink, L.J.D., Salinger, A.G.: Two- and three-dimensional nonlocal density functional theory for inhomogeneous fluids: I. Algorithms and parallelization. J. Comput. Phys. **159**, 407–424 (2000)

16. Frink, L.J.D., Salinger, A.G., Sears, M.P., Weinhold, J.D., Frischknecht, A.L.: Numerical challenges in the application of density functional theory to biology and nanotechnology. J. Phys. **14**, 12167–12187 (2002)

17. Frydel, D., Levin, Y.: A close look into the excluded volume effects within a double layer. J. Chem. Phys. **137**, 164703 (2012)

18. Gillespie, D.: A review of steric interactions of ions: why some theories succeed and others fail to account for ion size. Microfluid. Nanofluid. **18**, 717–738 (2014)

19. Gillespie, D., Nonner, W., Eisenberg, R.S.: Coupling Poisson–Nernst–Planck and density functional theory to calculate ion flux. J. Phys. **14**, 12129–12145 (2002)

20. Gillespie, D., Nonner, W., Eisenberg, R.S.: Density functional theory of charged, hard-sphere fluids. Phys. Rev. E **68**, 031503 (2003)

21. Hansen, J., McDonald, I.: Theory of Simple Liquids, 3rd edn. Academic Press, Cambridge (2006)

22. Hansen-Goos, H., Mecke, K.: Fundamental measure theory for inhomogeneous fluids of nonspherical hard particles. Phys. Rev. Lett. **102**, 018302 (2009)

23. Harris, R.C., Bredenberg, J.H., Silalahi, A.R.J., Boschitsch, A.H., Fenley, M.O.: Understanding the physical basis of the salt dependence of the electrostatic binding free energy of mutated charged ligand-nucleic acid complexes. Biophys. Chem. **156**, 79–87 (2011)

24. Harris, R.C., Boschitsch, A.H., Fenley, M.O.: Sensitivities to parameterization in the size-modified Poisson–Boltzmann equation. J. Chem. Phys. **140**, 075102 (2014)

25. Horng, T.L., Lin, T.C., Liu, C., Eisenberg, B.: PNP equations with steric effects: a model of ion flow through channels. J. Phys. Chem. B **116**, 11422–11441 (2012)

26. Hyon, Y., Eisenberg, B., Liu, C.: A mathematical model for the hard sphere repulsion in ionic solutions. Commun. Math. Sci. **9**, 459–475 (2011)

27. Im, W., Roux, B.: Ion permeation and selectivity of ompf porin: a theoretical study based on molecular dynamics, brownian dynamics, and continuum electrodiffusion theory. J. Mol. Biol. **322**(4), 851–869 (2002)

28. Ji, S., Liu, W.: Poisson–Nernst–Planck systems for ion flow with density functional theory for hard-sphere potential: I–V relations and critical potentials. Part I: analysis. J. Dyn. Differ. Equ. **24**, 955–983 (2012)

29. Jiang, J., Cao, D., De Jiang, WuJ: Time-dependent density functional theory for ion diffusion in electrochemical systems. J. Phys. **26**, 284102 (2014)

30. Jimenez-Morales, D., Liang, J., Eisenberg, B.: Ionizable side chains at catalytic active sites of enzymes. Eur. Biophys. J. **41**, 449–460 (2012)

31. Kamalvand, M., Keshavarzi, T.E., Mansoori, G.A.: Behavior of the confined hard-sphere fluid within nanoslits: a fundamental-measure density-functional theory study. Int. J. Nanosci. **07**, 245–253 (2008)

32. Kierlik, E., Rosinberg, M.L.: Free-energy density functional for the inhomogeneous hard-sphere fluid: application to interfacial adsorption. Phys. Rev. A **42**, 3382–3387 (1990)

33. Kilic, M.S., Bazant, M.Z., Ajdari, A.: Steric effects in the dynamics of electrolytes at large applied voltages I: double-layer charging. Phys. Rev. E **75**, 021502 (2007)

34. Knepley, M.G., Karpeev, D.A., Davidovits, S., Eisenberg, R.S., Gillespie, D.: An efficient algorithm for classical density functional theory in three dimensions: ionic solutions. J. Chem. Phys. **132**, 124101 (2010)
35. Kurnikova, M.G., Coalson, R.D., Graf, P., Nitzan, A.: A lattice relaxation algorithm for three-dimensional Poisson–Nernst–Planck theory with application to ion transport through the gramicidin A channel. Biophys. J. **76**, 642–656 (1999)
36. Levesque, M., Vuilleumier, R., Borgis, D.: Scalar fundamental measure theory for hard spheres in three dimensions: application to hydrophobic solvation. J. Chem. Phys. **137**, 034115 (2012)
37. Li, B., Liu, P., Xu, Z., Zhou, S.: Ionic size effects: generalized Boltzmann distributions, counterion stratification and modified Debye length. Nonlinearity **26**, 2899–2922 (2013)
38. Lin, G., Liu, W., Yi, Y., Zhang, M.: Poisson–Nernst–Planck systems for ion flow with a local hard-sphere potential for ion size effects. SIAM J. Appl. Dyn. Syst. **12**, 1613–1648 (2013)
39. Liu, J.L.: Numerical methods for the Poisson–Fermi equation in electrolytes. J. Comput. Phys. **247**, 88–99 (2013)
40. Liu, J.L., Eisenberg, B.: Correlated ions in a calcium channel model: a Poisson–Fermi theory. J. Phys. Chem. B **117**, 12051–12058 (2013)
41. Liu, J.L., Eisenberg, B.: Poisson–Nernst–Planck-Fermi theory for modeling biological ion channels. J. Chem. Phys. **141**, 22D532 (2014)
42. Liu, W., Tu, X., Zhang, M.: Poisson–Nernst–Planck systems for ion flow with density functional theory for hard-sphere potential: I–V relations and critical potentials. Part II: numerics. J. Dyn. Differ. Equ. **24**, 985–1004 (2012)
43. Lu, B., Zhou, Y.: Poisson–Nernst–Planck equations for simulating biomolecular diffusion-reaction processes II: size effects on ionic distributions and diffusion-reaction rates. Biophys. J. **100**, 2475–2485 (2011)
44. Lu, B., Zhou, Y., Huber, G.A., Bond, S.D., Holst, M.J., McCammon, J.A.: Electrodiffusion: a continuum modeling framework for biomolecular systems with realistic spatiotemporal resolution. J. Chem. Phys. **127**, 135102 (2007)
45. Lu, B., Zhou, Y., Holst, M.J., McCammon, J.A.: Recent progress in numerical methods for the Poisson–Boltzmann equation in biophysical applications. Commun. Comput. Phys. **3**, 973–1009 (2008)
46. Meng, D., Zheng, B., Lin, G., Sushko, M.L.: Numerical solution of 3D Poisson–Nernst–Planck equations coupled with classical density functional theory for modeling ion and electron transport in a confined environment. Commun. Comput. Phys. **16**, 1298–1322 (2014)
47. Nauman, E., He, D.Q.: Nonlinear diffusion and phase separation. Chem. Eng. Sci. **56**, 1999–2018 (2001)
48. Phan, S., Kierlik, E., Rosinberg, M.L., Bildstein, B., Kahl, G.: Equivalence of two free-energy models for the inhomogeneous hard-sphere fluid. Phys. Rev. E **48**, 618–620 (1993)
49. Pods, J., Schönke, J., Bastian, P.: Electrodiffusion models of neurons and extracellular space using the Poisson–Nernst–Planck equations-numerical simulation of the intra- and extracellular potential for an axon model. Biophys. J. **105**, 242–254 (2013)
50. Qiao, Y., Tu, B., Lu, B.: Ionic size effects to molecular solvation energy and to ion current across a channel resulted from the nonuniform size-modified PNP equations. J. Chem. Phys. **140**, 174102 (2014)
51. Rosenfeld, Y.: Free-energy model for the inhomogeneous hard-sphere fluid mixture and density-functional theory of freezing. Phys. Rev. Lett. **63**, 980–983 (1989)
52. Rosenfeld, Y.: Free-energy model for the inhomogeneous hard-sphere fluid in D dimensions: structure factors for the hard-disk (D = 2) mixtures in simple explicit form. Phys. Rev. A **42**, 5978–5989 (1990)
53. Rosenfeld, Y.: Free energy model for inhomogeneous fluid mixtures: Yukawa-charged hard spheres, general interactions, and plasmas. J. Chem. Phys. **98**, 8126–8148 (1993)
54. Rosenfeld, Y.: Density functional theory of molecular fluids: free-energy model for the inhomogeneous hard-body fluid. Phys. Rev. E **50**, R3318–R3321 (1994)
55. Rosenfeld, Y.: Free energy model for the inhomogeneous hard-body fluid: application of the Gauss–Bonnet theorem. Mol. Phys. **86**, 637–647 (1995)
56. Rosenfeld, Y., Levesque, D., Weis, J.J.: Free-energy model for the inhomogeneous hard-sphere fluid mixture: triplet and higher-order direct correlation functions in dense fluids. J. Chem. Phys. **92**, 6818–6832 (1990)
57. Rosenfeld, Y., Schmidt, M., Löwen, H., Tarazona, P.: Dimensional crossover and the freezing transition in density functional theory. J. Phys. **8**, L577–L581 (1996)
58. Rosenfeld, Y., Schmidt, M., Löwen, H., Tarazona, P.: Fundamental-measure free-energy density functional for hard spheres: dimensional crossover and freezing. Phys. Rev. E **55**, 4245–4263 (1997)
59. Roth, R.: Fundamental measure theory for hard-sphere mixtures: a review. J. Phys. **22**, 063102 (2010)
60. Roth, R., Evans, R., Lang, A., Kahl, G.: Fundamental measure theory for hard-sphere mixtures revisited: the White Bear version. J. Phys. **14**, 12063–12078 (2002)

61. Santangelo, C.D.: Computing counterion densities at intermediate coupling. Phys. Rev. E **73**, 041512 (2006)
62. Sears, M.P., Frink, L.J.D.: A new efficient method for density functional theory calculations of inhomogeneous fluids. J. Comput. Phys. **190**, 184–200 (2003)
63. Si, H.: TetGen, a delaunay-based quality tetrahedral mesh generator. ACM Trans. Math. Softw. **41**, 11:1–11:36 (2015)
64. Silalahi, A.R.J., Boschitsch, A.H., Harris, R.C., Fenley, M.O.: Comparing the predictions of the nonlinear Poisson–Boltzmann equation and the ion size-modified Poisson–Boltzmann equation for a low-dielectric charged spherical cavity in an aqueous salt solution. J. Chem. Theory Comput. **6**, 3631–3639 (2010)
65. Tarazona, P.: Density functional for hard sphere crystals: a fundamental measure approach. Phys. Rev. Lett. **84**, 694–697 (2000)
66. Tarazona, P., Rosenfeld, Y.: From zero-dimension cavities to free-energy functionals for hard disks and hard spheres. Phys. Rev. E **55**, R4873–R4876 (1997)
67. Tarazona, P., Rosenfeld, Y.: Free energy density functional from 0d cavities. New Approaches to Problems in Liquid State Theory, vol. 529, pp. 293–302. Springer, Netherlands (1999)
68. Tu, B., Chen, M., Xie, Y., Zhang, L., Eisenberg, B., Lu, B.: A parallel finite element simulator for ion transport through three-dimensional ion channel systems. J. Comput. Chem. **34**, 2065–2078 (2013)
69. Xie, Y., Cheng, J., Lu, B., Zhang, L.: Parallel adaptive finite element algorithms for solving the coupled electro-diffusion equations. Mol. Based Math. Biol. **1**, 90–108 (2013)
70. Yu, Y., Wu, J.: Structures of hard-sphere fluids from a modified fundamental-measure theory. J. Chem. Phys. **117**, 10156–10164 (2002)
71. Zhang, L.: A parallel algorithm for adaptive local refinement of tetrahedral meshes using bisection. Numer. Math. Theory Methods Appl. **2**, 65–89 (2009)